stack may be weakly dimerized by van der Waals forces with the alternating distances between neighboring planar complexes in the stack being 3.77 (1) and 3.96 (1) Å (measured as the distance from the midpoint between the platinum atoms of one complex to the best plane of neighboring binuclear species, i.e., plane 8 in Table III).

Two different types of interaction might be invoked to rationalize the overall planarity of this complex. The weak van der Waals dimerization noted above may contribute to stabilization of the planar structure. This interaction appears not to involve direct metal–metal overlap since the shortest platinum–platinum distance between nearest-neighbor metal atoms in adjacent molecules in 4.028 (2) Å. The closest atom contact between the molecules occurs for the bridging ligands (Cl⁻ and the nitrogen atoms of pz) of nearest neighbors; however, this interaction is at a relatively long distance (3.74 (2) Å) compared to the sum of van der Waals radii for nitrogen and chlorine. Thus on balance, this interaction appears to be relatively weak and probably is not the sole driving force for planarity. The second type of interaction favoring planarity involves the potential of the pyrazolide ligand to function as a π-*donor* group via the filled π orbitals of the ring. As noted above, the platinum-to-carbon and -nitrogen bond distances

are not significantly shorter than those of other related complexes; therefore, strong structural support for this type of interaction is lacking. We have, however, observed that the barrier to olefin rotation is higher in the title complex[13] than in the mononuclear species *trans*-PtCl$_2$(C$_2$H$_4$)(C$_3$H$_4$N$_2$). The higher barrier to olefin rotation in the binuclear complex may indicate a synergistic enhancement of the platinum-olefin π bond due to ligand-to-metal π donation by the pyrazolide group.

(13) Johnson, D. A.; Deese, W. C., unpublished results.

Contribution from the Chemistry Department, Brookhaven National Laboratory, Upton, New York 11973, and the Department of Chemistry, Georgetown University, Washington, D.C. 20007

Crystal and Molecular Structures of Pentaammine(pyrazine)ruthenium(II) Tetrafluoroborate and Pentaammine(pyrazine)ruthenium(III) Trifluoromethanesulfonate Monohydrate

MARY E. GRESS, CAROL CREUTZ,* and CARL O. QUICKSALL

For [Ru(NH$_3$)$_5$(C$_4$N$_2$H$_4$)](BF$_4$)$_2$ the space group is $P2_12_12_1$ with cell parameters a = 12.615 (2) Å, b = 15.610 (3) Å, c = 7.965 (2) Å, and Z = 4. For [Ru(NH$_3$)$_5$(C$_4$N$_2$H$_4$)](CF$_3$SO$_3$)$_3$·H$_2$O the space group is *Pnma* with cell parameters a = 23.795 (4) Å, b = 8.062 (2) Å, c = 12.848 (2) Å, and Z = 4. The geometries of both the Ru(NH$_3$)$_5$pz^{2+} (pz = pyrazine) and Ru(NH$_3$)$_5$pz^{3+} cations are approximately octahedral, with the plane of the pyrazine ring intersecting at a 45° angle the equatorial plane containing the bound pyrazine N and the three N atoms of the NH$_3$ groups, as is expected from steric considerations. The Ru–NH$_3$ bond lengths are similar to those found in other ammine complexes: Ru(II)–NH$_3$, 2.15–2.17 Å; Ru(III)–NH$_3$, 2.10–2.13 Å. By contrast the Ru(II)–pz bond (2.006 Å) is shorter than the Ru(III)–pz bond (2.076 Å) by 0.07 Å. This is attributed to π back-bonding between Ru(II) and pyrazine. The dimensions of the mononuclear ions Ru(NH$_3$)$_5$pz^{2+} and Ru(NH$_3$)$_5$pz^{3+} are used to model the structure of valence-localized Ru^{II}(NH$_3$)$_5$pzRu^{III}(NH$_3$)$_5$$^{5+}$. The observed properties of this ion are then compared with those predicted from Marcus–Hush electron-transfer theory.

Introduction

Although the physical and chemical properties of mononuclear pentaammineruthenium(II) and -(III) complexes containing aromatic N heterocycles (Ru(NH$_3$)$_5$L^{2+} and Ru(NH$_3$)$_5$L^{3+}, L = pyridine, isonicotinamide, pyrazine, etc.), have been extensively investigated,[1-6] no structural data have been available for complexes of this class. It is especially desirable to compare bond length data for Ru(NH$_3$)$_5$L^{2+} and Ru(NH$_3$)$_5$L^{3+} with the same π acid L. This comparison is expected to provide additional information concerning the back-bonding interaction between L and the π base Ru(NH$_3$)$_5$$^{2+}$, which is manifested in the thermodynamic[4,5] and spectral[1,6] properties of Ru(NH$_3$)$_5$L^{2+}. Furthermore, the magnitudes of the bond lengths for such complexes in both oxidation states are of considerable interest in assessing the success of current electron-transfer theories. Biomolecular

self-exchange rates for Ru(NH$_3$)$_5$L^{2+}/Ru(NH$_3$)$_5$L^{3+} couples have now been experimentally evaluated[7] and can be compared with theoretical values if the dimensions of the ions are known.[8-10] Structural data bearing on the bond length differences between Ru(NH$_3$)$_5$L^{2+} and Ru(NH$_3$)$_5$L^{3+} are also of importance in the area of intramolecular-electron-transfer theory as studied through the physical properties of valence-trapped mixed-valence ions,[11] e.g., the series of mixed-valence

(1) Ford, P. C.; Rudd, D. F. P.; Gaunder, R.; Taube, H. *J. Am. Chem. Soc.* **1969**, *90*, 1187.
(2) Ford, P. C. *Coord. Chem. Rev.* **1970**, *5*, 75.
(3) Taube, H. *Surv. Progr. Chem.* **1973**, *6*, 1.
(4) Matsubara, T.; Ford, P. C. *Inorg. Chem.* **1976**, *15*, 1107.
(5) Shepherd, R. E.; Taube, H. *Inorg. Chem.* **1973**, *12*, 1392.
(6) Zwickel, A. M.; Creutz, C. *Inorg. Chem.* **1971**, *10*, 2395.
(7) Brown, G. M.; Krentzien, H. J.; Abe, M.; Taube, H. *Inorg. Chem.* **1979**, *18*, 3374.
(8) Sutin, N. *Bioinorg. Chem.* **1973**, *2*, 611.
(9) Marcus, R. A. *Discuss. Faraday Soc.* **1960**, *29*, 11; *Electrochim. Acta* **1968**, *13*, 995.
(10) Brown, G. M.; Sutin, N. *J. Am. Chem. Soc.* **1979**, *101*, 883.

*To whom correspondence should be addressed at Brookhaven National Laboratory.

Table I. Crystal Data for [Ru(NH$_3$)$_5$pz](BF$_4$)$_2$ and [Ru(NH$_3$)$_5$pz](CF$_3$SO$_3$)$_3$·H$_2$O

	Ru(II)	Ru(III)
space group	$P2_12_12_1$	*Pnma*
fw	440.93	732.54
a, Å	12.615 (2)	23.795 (4)
b, Å	15.610 (3)	8.062 (2)
c, Å	7.965 (2)	12.848 (2)
vol, Å^3	1568.5	2464.7
Z	4	4
D_c, g cm^{-3}	1.868	1.975
D_m (by flotation in C$_2$H$_4$Br$_2$/CCl$_4$), g cm^{-3}	1.86 (1)	1.96 (1)

complexes (NH$_3$)$_5$Ru^{II}–L–Ru^{III}(NH$_3$)$_5^{5+}$ (L = 4,4'-bipyridine, dipyridylethane, etc.) studied by Taube and coworkers.[12] Structural data for the mononuclear fragments (Ru(NH$_3$)$_5$L) provide a touchstone for the interpretation of observations on these binuclear ions since the mononuclear complexes represent the limit of zero electronic interaction between the two metal centers. For these reasons structural studies of the penta-ammine(pyrazine)ruthenium complexes were undertaken. The results obtained for [Ru(NH$_3$)$_5$pz](BF$_4$)$_2$ (pz = pyrazine) and [Ru(NH$_3$)$_5$pz](CF$_3$SO$_3$)$_3$·H$_2$O are reported below.

Experimental Section

The complex [Ru(NH$_3$)$_5$pz](BF$_4$)$_2$ (I) was prepared as described in the literature.[1] Crystals were obtained by slowly cooling a saturated aqueous solution prepared at ~50 °C. Ru(NH$_3$)$_5$pz^{3+} was prepared by oxidation of [Ru(NH$_3$)$_5$pz](ClO$_4$)$_2$ dissolved in 0.1 M CF$_3$SO$_3$H with saturated Br$_2$ water. An equal volume of concentrated tri-fluoromethanesulfonic acid (~4 M) was added to the above solution, and after filtration, the yellow solution was left in the refrigerator (5 °C) for several days. Light orange crystals of [Ru(NH$_3$)$_5$pz]-(CF$_3$SO$_3$)$_3$·H$_2$O (II) were collected after that time.

Preliminary precession photographs of I indicated the space group $P2_12_12_1$ by *mmm* diffraction symmetry and systematic absences $h00$ ($h = 2n + 1$), $0k0$ ($k = 2n + 1$), and $00l$ ($l = 2n + 1$). Precession photographs of II also exhibited *mmm* diffraction symmetry, with systematic absences $0kl$ ($k + l = 2n + 1$) and $hk0$ ($h = 2n + 1$), indicating space group *Pnma* or *Pn2$_1$a*.

The cell parameters and intensity data were measured at room temperature (22 °C) by θ–2θ scans on an automated Enraf-Nonius CAD-4 diffractometer using Mo Kα (λ = 0.710 69 Å) radiation. Cell parameters, given in Table I, were determined by least-squares re-finement of 25 well-distributed high-order reflections centered at $\pm2\theta$. The experimental conditions and data refinement are summarized in Table II. The data were corrected for Lorentz–polarization effects and for absorption by using the analytical absorption method of DeMeulenaer and Tompa.[13] The structures were solved by employing both Patterson and direct methods.[14] Refinement was carried out by full-matrix least squares methods using the Hartree-Fock scattering factors of Cromer and Mann,[15] with those of Ru and S modified for the real and imaginary parts of anomalous dispersion.[16] The function minimized was $\sum w[|F_o| - k|F_c|]^2$, where w^{-1} is defined as $[\sigma_c^2(F_o)^2 + (aF_o^2)^2]/4F_o^2$; σ_c was from counting statistics and $a = 0.02$ for I and $a = 0.04$ for II.

Since I crystallized in the noncentrosymmetric space group $P2_12_12_1$, it was necessary to determine the enantiomeric form. Least-squares refinement of the enantiomorph, obtained by inverting the coordinates ($x, y, z \rightarrow -x, -y, -z$), gave poorer results ($R = 0.066, R_w = 0.060,$
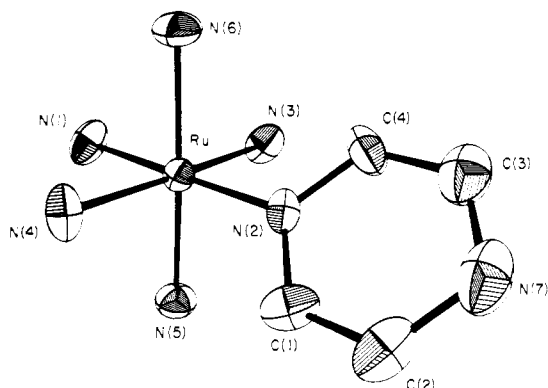

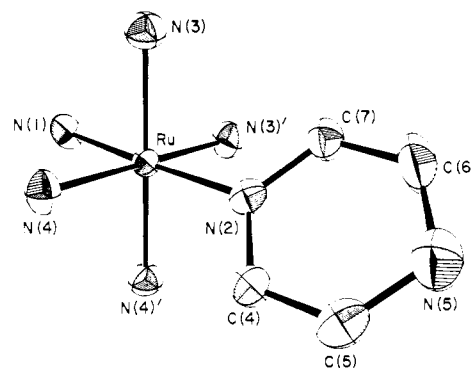**Figure 1.** View of the Ru(NH$_3$)$_5$pz^{2+} cation. Atoms are represented as 50% probability ellipsoids.

Figure 2. View of the Ru(NH$_3$)$_5$pz^{3+} cation drawn with 50% probability ellipsoids. Primed atoms are related to unprimed atoms by a mirror plane.

and S = 1.593). Refinement of II was also carried out in the lower order space group *Pn2$_1$a*. This refinement was no more satisfactory, and the results are reported from the *Pnma* refinement. The somewhat poorer refinement of structure II than that of I is most likely due to difficulty in obtaining accurate data from a thin plate-shaped crystal.

The final positional and thermal parameters and their standard deviations are given in Tables III and IV. Selected interatomic distances and angles and their standard deviations are given in Tables V and VI. Lists of observed and calculated structure factors are available as supplementary material.

Description and Discussion of the Structures

The geometries of both the Ru(NH$_3$)$_5$pz^{2+} and Ru-(NH$_3$)$_5$pz^{3+} cations are, as expected, close to octahedral as shown in the ORTEP drawings, Figures 1 and 2. In both ions the Ru–pz bond is shorter than the Ru–NH$_3$ bonds, and, in both, the plane of the pyrazine ring intersects at a 45° angle the equatorial plane containing the pyrazine N atom and the three N atoms of the NH$_3$ groups, as would be predicted from stereochemical considerations. In fact, taken as a whole, the structures are strikingly similar. In II the pyrazine ring lies on a mirror plane; in I the deviation of any atom in the py-razine ring from the plane defined by $-0.7041x + 0.4242y + 0.5695z - 1.3896 = 0$ is less than 0.01 Å. Thus in both cations the pyrazine ring is planar as is free pyrazine.[17] In free pyrazine, as well as in silver(I) pyrazine nitrate,[18] the C–C bonds are longer (0.01–0.02 Å) than the C–N bonds, but in neither of the present structures is a significant ($\geq3\sigma$) lengthening of these bonds observed.

The crystal structure of I consists of alternating layers of Ru(NH$_3$)$_5$pz^{2+} cations and BF$_4^-$ anions perpendicular to the a axis. Although the ammine hydrogen atom positions could

(11) Hush, N. S. *Porg. Inorg. Chem.* **1967**, *8*, 357.
(12) Taube, H. *Ann. N.Y. Acad. Sci.* **1978**, *313*, 481 and references cited therein.
(13) Templeton, L. K.; Templeton, D. H. Abstracts of the American Crys-tallographic Association Meeting, Storrs, Conn., 1973; No. E10.
(14) Programs used for the structure solutions and refinements included the CRYSNET library programs at BNL, the ALFF Fourier program by Hubbard, Quicksall, and Jacobson, MULTAN direct-methods program by Germain, Main, and Woolfson, and Johnson's ORTEP2 plotting pro-gram.
(15) Cromer, D. T.; Mann, J. B. *Acta Crystallogr., Sect. A* **1968**, *A24*, 321.
(16) Lonsdale, K., Ed. "International Tables for X-ray Crystallography", 2nd ed.; Kynoch Press: Birmingham, England, 1968; Vol. III, p 215.

(17) Wheatley, P. J. *Acta Crystallogr.* **1957**, *10*, 182.
(18) Vranka, R. G.; Amma, E. L. *Inorg. Chem.* **1966**, *5*, 1020.

Table II. Experimental and Structural Refinement Data

	$[Ru(NH_3)_5pz](BF_4)_2$	$[Ru(NH_3)_5pz](CF_3SO_3)_3 \cdot H_2O$
cryst description		
color	deep red	pale orange
cryst faces and dist from center, mm	(010), (0$\bar{1}$0), 0.105; (120), ($\bar{1}$20),	(10$\bar{1}$), ($\bar{1}$01), 0.033; (0$\bar{1}$0), 0.15;
	(1$\bar{2}$0), ($\bar{1}\bar{2}$0), 0.096; (10$\bar{1}$), ($\bar{1}$0$\bar{1}$),	($\bar{1}$00), 0.09; ($\bar{5}$11), (216), (2$\bar{1}$0),
	0.175; (001), 0.194; ($\bar{2}$03), 0.210	0.11; (101), 0.10
vol, mm³	0.0146	0.00475
data collection		
radiation	Mo Kα, graphite monochromated	Mo Kα, filtered with Nb foil
2θ limits, deg	1–60	1–64
scan width, deg	$0.90 + 0.35 \tan\theta$	$0.70 + 0.35 \tan\theta$
no. of unique reflctns measd	3484	4511
abs cor		
linear abs coeff, cm^{-1}	10.72	10.03
max cor to F^2	1.296	1.231
min cor to F^2	1.174	1.062
least-squares refinement		
data with $F_o > 3\sigma(F_o)$	2808	2334
no. of parameters	199	199
$R = \Sigma |F_o - kF_c|/\Sigma |F_o|$	0.064	0.088
$R_w = \{\Sigma[w(F_o - kF_c)]^2/\Sigma wF_o^2\}^{1/2}$	0.058	0.076
goodness of fit, $S = \{w(F_o - kF_c)]^2/(N_o - N_v)\}^{1/2}$	1.550	1.345

Table III. Fractional Atomic Coordinates and Thermal Parameters $(\times 10^4)^a$ for $[Ru(NH_3)_5pz](BF_4)_2$[b]

atom	x	y	z	β_{11}	β_{22}	β_{33}	β_{12}	β_{13}	β_{23}
Ru	0.01817 (5)	0.13233 (4)	0.15482 (8)	34.3 (3)	21.2 (2)	81.3 (8)	−0.3 (3)	1.8 (6)	0.2 (5)
N(1)	0.0173 (9)	0.0238 (4)	0.3244 (9)	67 (5)	31 (3)	145 (14)	7 (4)	26 (10)	21 (6)
N(2)	0.0166 (8)	0.2335 (4)	−0.0005 (7)	43 (4)	26 (3)	70 (9)	4 (4)	5 (7)	5 (4)
N(3)	0.0245 (9)	0.0439 (4)	−0.0518 (9)	67 (6)	25 (3)	133 (13)	−11 (4)	22 (9)	−14 (5)
N(4)	0.0116 (9)	0.2164 (4)	0.3708 (8)	74 (6)	35 (3)	80 (11)	5 (4)	0 (8)	−4 (5)
N(5)	0.1881 (5)	0.1329 (5)	0.1647 (11)	34 (4)	39 (3)	157 (14)	−1 (4)	−10 (7)	12 (13)
N(6)	−0.1522 (5)	0.1267 (5)	0.1541 (12)	26 (4)	50 (4)	178 (15)	2 (4)	0 (7)	6 (15)
N(7)	0.0105 (7)	0.3764 (5)	−0.2212 (9)	68 (6)	44 (4)	163 (14)	18 (5)	27 (8)	33 (7)
C(1)	0.0805 (7)	0.3043 (5)	0.0201 (12)	46 (6)	19 (3)	173 (18)	−1 (3)	19 (9)	−15 (7)
C(2)	0.0785 (7)	0.3731 (6)	−0.0862 (12)	56 (6)	23 (4)	196 (19)	9 (5)	38 (9)	12 (8)
C(3)	−0.0513 (7)	0.3076 (6)	−0.2426 (12)	57 (7)	42 (5)	137 (17)	12 (5)	20 (9)	13 (8)
C(4)	−0.0482 (6)	0.2376 (6)	−0.1369 (11)	43 (5)	49 (5)	82 (13)	12 (4)	−14 (7)	0 (7)
B(1)	0.2494 (9)	0.3943 (7)	0.3676 (17)	64 (8)	32 (5)	126 (23)	11 (5)	−7 (11)	0 (9)
F(1)	0.2680 (8)	0.4236 (6)	0.2085 (10)	192 (10)	90 (5)	163 (16)	−1 (6)	25 (10)	41 (8)
F(2)	0.2416 (5)	0.3061 (4)	0.3644 (12)	115 (6)	32 (3)	347 (20)	−4 (3)	13 (11)	5 (8)
F(3)	0.3347 (7)	0.4141 (6)	0.4603 (12)	189 (10)	98 (6)	433 (26)	−60 (6)	−207 (14)	17 (11)
F(4)	0.1613 (7)	0.4294 (5)	0.4155 (15)	183 (10)	81 (5)	626 (36)	62 (6)	200 (16)	32 (11)
B(2)	0.7563 (10)	0.3793 (8)	0.3060 (17)	66 (8)	29 (5)	190 (27)	−7 (5)	−33 (12)	1 (10)
F(5)	0.7656 (9)	0.3100 (5)	0.2097 (13)	284 (14)	61 (5)	325 (24)	25 (7)	−43 (16)	−33 (9)
F(6)	0.7523 (5)	0.4479 (4)	0.2104 (11)	96 (6)	51 (3)	327 (23)	−15 (4)	−65 (10)	51 (20)
F(7)	0.6675 (8)	0.3729 (8)	0.3962 (14)	179 (10)	176 (10)	630 (37)	15 (9)	243 (16)	137 (20)
F(8)	0.8401 (7)	0.3824 (6)	0.4087 (12)	211 (10)	111 (6)	496 (28)	−59 (7)	−243 (15)	101 (12)

^{a} The form of the anisotropic thermal ellipsoid is $\exp[-(\beta_{11}h^2 + \beta_{22}k^2 + \beta_{33}l^2 + 2\beta_{12}hk + 2\beta_{13}hl + 2\beta_{23}kl)]$. ^{b} Numbers in parentheses in this and succeeding tables are estimated standard deviations in the least significant figures.

not be determined, numerous possibilities exist for hydrogen bonding between layers. Of the 12 interatomic nitrogen–fluorine distances less than 3.20 Å, the shortest are N(1)–F(3) (3.04 Å), N(6)–F(5) (3.05 Å), N(4)–F(7) (3.06 Å), and N(1)–F(4) (3.12 Å).

The crystal structure of II consists of layers of Ru(NH$_3$)$_5$pz^{3+} cations surrounded by CF$_3$SO$_3^-$ anions on the mirror planes perpendicular to the b axis. The crystallographic mirror plane through the anions would imply an exact staggered or eclipsed conformation, and the conformations of the three unique anions, as expected, are staggered. The water oxygens, which also lie on the mirror plane, have closest intermolecular contacts of 2.94 Å to O(22) and O(22)′, 3.07 Å to O(11), and 3.10 Å to N(3) and N(3)′.

The overall geometries of the two cations presumably are determined largely by steric rather than electronic factors. The effect of the charge of the metal center is apparent in the Ru–NH$_3$ bonds. The Ru(II)–NH$_3$ bond lengths range from 2.15 to 2.17 Å while the Ru(III)–NH$_3$ bond lengths range from 2.10 to 2.13 Å. In Table VII these may be compared

with Ru–N bond lengths recorded for other saturated amines. It is notable that the Ru(II)–NH$_3$ bonds in I are somewhat longer than those in Ru(NH$_3$)$_6^{2+}$ (2.144 (4) Å). Similarly the Ru(III)–NH$_3$ bonds in II are slightly longer than those in Ru(NH$_3$)$_6^{3+}$ (2.104 (4) Å). In contrast to the small trans effect reported for *cis*-[Ru(NH$_3$)$_4$(isn)$_2$](ClO$_4$)$_2$ (isn = isonicotinamide) our results provide no unequivocal evidence for lengthening of the Ru–NH$_3$ bond trans to the pyrazine in I.

The operation of electronic factors is, however, evident in the pattern of metal–pyrazine bond lengths observed. That obtained for Ru(II) (2.006 (6) Å) is shorter by 0.07 Å than that found for Ru(III) (2.076 (8) Å). This is contrary to the trend expected from metal charge, but is expected from the high affinity of Ru(NH$_3$)$_5^{2+}$ for π-acceptor ligands. A similar effect was noted for the tetraammine pair Ru(NH$_3$)$_4$(isn)$_2^{2+/3+}$ in which the Ru(II)–isn bond length is 2.060 (4) Å (Table VII) while that for Ru(III)–isn is 2.099 (4) Å ($\Delta r = 0.039$ Å). Analogous consequences of $d\pi{-}\pi^*$ back-bonding are reflected in the Fe(CN)$_6^{4-}$/Fe(CN)$_6^{3-}$ pair; the Fe(II)–C bond is 0.026 (8) Å shorter than the Fe(III)–C bond.[19]

Table IV. Fractional Atomic Coordinates and Thermal Parameters $(\times 10^4)^a$ $[Ru(NH_3)_5pz](CF_3SO_3)_3 \cdot H_2O^b$

atom	x	y	z	β_{11}	β_{22}	β_{33}	β_{12}	β_{13}	β_{23}
Ru	0.63844 (3)	0.2500^b	0.17916 (6)	8.3 (1)	66.9 (10)	27.6 (4)	0	−0.5 (3)	0
S(1)	0.4378 (1)	0.2500	0.6599 (2)	12 (1)	95 (4)	46 (2)	0	5 (1)	0
S(2)	0.9386 (1)	0.2500	0.3737 (2)	14 (1)	151 (6)	54 (2)	0	−1 (1)	0
S(3)	0.2573 (1)	0.2500	0.9802 (2)	15 (1)	75 (4)	51 (2)	0	11 (1)	0
N(1)	0.5743 (4)	0.2500	0.2943 (6)	8 (2)	210 (21)	32 (5)	0	4 (2)	0
N(2)	0.6987 (3)	0.2500	0.0623 (6)	11 (2)	48 (12)	41 (5)	0	0 (2)	0
N(5)	0.7799 (5)	0.2500	−0.0957 (8)	18 (2)	152 (20)	47 (7)	0	5 (3)	0
C(1)	0.5076 (6)	0.2500	0.6031 (12)	18 (3)	214 (32)	70 (11)	0	4 (4)	0
C(2)	0.8913 (8)	0.2500	0.2624 (12)	24 (4)	276 (38)	64 (12)	0	−11 (5)	0
C(3)	0.1841 (7)	0.2500	0.9433 (11)	18 (3)	229 (32)	57 (10)	0	0 (4)	0
C(4)	0.7552 (4)	0.2500	0.0836 (8)	9 (2)	130 (19)	36 (6)	0	2 (3)	0
C(5)	0.7941 (4)	0.2500	0.0050 (9)	10 (2)	121 (21)	58 (8)	0	3 (3)	0
C(6)	0.7243 (6)	0.2500	−0.1156 (9)	19 (3)	279 (35)	28 (7)	0	5 (4)	0
C(7)	0.6836 (5)	0.2500	−0.0394 (8)	12 (2)	122 (19)	32 (6)	0	2 (3)	0
F(11)	0.5069 (5)	0.2500	0.5026 (8)	39 (3)	541 (42)	56 (6)	0	23 (3)	0
O(11)	0.4449 (5)	0.2500	0.7693 (8)	25 (3)	304 (28)	72 (9)	0	9 (4)	0
F(21)	0.9188 (5)	0.2500	0.1755 (8)	38 (3)	832 (59)	52 (6)	0	13 (4)	0
O(21)	0.9015 (4)	0.2500	0.4614 (7)	18 (2)	265 (24)	58 (7)	0	6 (3)	0
F(31)^c	0.1736 (6)	0.2500	0.8552 (9)	30 (3)	1837 (131)	55 (8)	0	−7 (4)	0
O(31)	0.2562 (5)	0.2500	1.0870 (10)	19 (2)	671 (59)	89 (10)	0	15 (4)	0
O(W)	0.0501 (5)	0.2500	0.5917 (8)	25 (2)	338 (30)	62 (8)	0	15 (3)	0
N(3)	0.5948 (3)	0.4406 (8)	0.1009 (5)	16 (1)	99 (11)	48 (4)	3 (3)	−2 (2)	16 (5)
N(4)	0.6818 (3)	0.4384 (8)	0.2589 (5)	13 (1)	109 (11)	42 (4)	−5 (3)	0 (2)	−13 (5)
F(12)	0.5372 (3)	0.3769 (15)	0.6362 (7)	25 (2)	544 (33)	199 (10)	−70 (6)	18 (3)	−108 (14)
O(12)	0.4130 (3)	0.3980 (8)	0.6203 (5)	17 (1)	89 (9)	116 (6)	8 (3)	6 (2)	16 (6)
F(22)	0.8582 (3)	0.3789 (14)	0.2647 (7)	34 (2)	476 (28)	150 (8)	38 (7)	−27 (3)	57 (12)
O(22)	0.9711 (3)	0.3986 (12)	0.3603 (6)	21 (2)	248 (19)	128 (8)	−33 (5)	−5 (3)	46 (9)
F(32)	0.1542 (4)	0.3687 (16)	0.9849 (9)	27 (2)	498 (32)	258 (13)	38 (7)	−8 (4)	−131 (15)
O(32)	0.2791 (4)	0.3953 (13)	0.9341 (10)	28 (2)	232 (20)	224 (12)	−29 (6)	7 (5)	120 (12)

^{a} The form of the anisotropic thermal ellipsoid is $\exp[-(\beta_{11}h^2 + \beta_{22}k^2 + \beta_{33}l^2 + 2\beta_{12}hk + 2\beta_{13}hl + 2\beta_{23}kl)]$. ^{b} Parameters with no cited standard deviations are fixed by symmetry. ^{c} Low accuracy is due to rotational disorder.

Table V. Selected Bond Distances and Angles for $[Ru(NH_3)_5pz](BF_4)_2$

Distances, Å

Ru–N(1)	2.166 (7)	N(2)–C(1)	1.38 (1)
Ru–N(2)	2.006 (6)	C(1)–C(2)	1.37 (1)
Ru–N(3)	2.149 (7)	C(2)–N(7)	1.38 (1)
Ru–N(4)	2.165 (6)	N(7)–C(3)	1.34 (1)
Ru–N(5)	2.145 (6)	C(3)–C(4)	1.38 (1)
Ru–N(6)	2.151 (6)	C(4)–N(2)	1.36 (1)
B(1)–F(1)	1.37 (1)	B(2)–F(5)	1.33 (1)
B(1)–F(2)	1.38 (1)	B(2)–F(6)	1.32 (1)
B(1)–F(3)	1.34 (1)	B(2)–F(7)	1.33 (1)
B(1)–F(4)	1.30 (1)	B(2)–F(8)	1.34 (1)

Angles, Deg

N(2)–Ru–N(5)	91.7 (4)	N(3)–Ru–N(1)	88.6 (3)
N(2)–Ru–N(6)	91.2 (4)	N(1)–Ru–N(4)	88.7 (3)
N(2)–Ru–N(1)	179.0 (5)	N(3)–Ru–N(4)	177.3 (3)
N(2)–Ru–N(3)	91.9 (3)	C(1)–N(2)–C(4)	114.1 (7)
N(2)–Ru–N(4)	90.7 (2)	C(2)–N(7)–C(3)	115.6 (8)
N(5)–Ru–N(6)	177.1 (3)	N(2)–C(1)–C(2)	123.0 (9)
N(5)–Ru–N(1)	89.2 (4)	C(1)–C(2)–N(7)	121.7 (9)
N(5)–Ru–N(3)	89.6 (4)	C(4)–C(3)–N(7)	122.8 (9)
N(5)–Ru–N(4)	90.4 (4)	N(2)–C(4)–C(3)	122.8 (9)
N(6)–Ru–N(1)	88.0 (4)	Ru–N(2)–C(1)	123.5 (6)
N(6)–Ru–N(3)	90.5 (4)	Ru–N(2)–C(4)	122.4 (6)
N(6)–Ru–N(4)	89.4 (4)		

Table VI. Selected Bond Distances and Angles for $[Ru(NH_3)_5pz](CF_3SO_3)_3 \cdot H_2O$

Distances, Å

Ru–N(1)	2.125 (8)	Ru–N(3)	2.110 (6)
Ru–N(2)	2.076 (8)	Ru–N(4)	2.102 (6)
N(2)–C(4)	1.37 (1)	N(5)–C(6)	1.35 (2)
C(4)–C(5)	1.37 (1)	C(6)–C(7)	1.38 (1)
C(5)–N(5)	1.34 (1)	C(7)–N(2)	1.35 (1)
S(1)–C(1)	1.81 (2)	C(1)–F(11)	1.29 (2)
S(1)–O(11)	1.42 (1)	C(1)–F(12)	1.31 (1)
S(1)–O(12)	1.43 (1)		
S(2)–C(2)	1.81 (2)	C(2)–F(21)	1.29 (2)
S(2)–O(21)	1.43 (1)	C(2)–F(22)	1.30 (1)
S(2)–O(22)	1.44 (1)		
S(3)–C(3)	1.80 (2)	C(3)–F(31)	1.16 (2)^a
S(3)–O(31)	1.37 (1)	C(3)–F(32)	1.31 (1)
S(3)–O(32)	1.41 (1)		

Angles, Deg

N(1)–Ru–N(2)	177.8 (3)	N(2)–Ru–N(4)	90.8 (2)
N(1)–Ru–N(3)	88.8 (2)	N(3)–Ru–N(4)	87.0 (2)
N(1)–Ru–N(4)	89.7 (2)		
Ru–N(2)–C(4)	122.1 (6)	Ru–N(2)–C(7)	120.9 (7)
C(7)–N(2)–C(4)	117 (1)	C(4)–C(5)–N(5)	123 (1)
C(5)–C(6)–C(7)	116 (1)	N(5)–C(6)–C(7)	124 (1)
N(2)–C(4)–C(5)	121 (1)	C(6)–C(7)–N(2)	120 (1)

^{a} Bond length is imprecisely determined due to rotational disorder.

The Ru(III)–L bond lengths in Table VII cluster about 2.08–2.10 Å, despite the fact that the ligands L include pz, isn, and bpy and the compounds include very different secondary ligands (NH_3, O^{2-}, NO_2^-). The Ru(II)–L bond lengths encompass a larger range—2.00–2.10 Å if the sterically hindered $Ru(py)_6^{2+}$ cation is included and 2.00–2.08 Å if the latter is omitted. Two comparisons are striking: the Ru(II)–isn bond length in *cis*-$Ru(NH_3)_4(isn)_2^{2+}$ (2.060 (4) Å) is not significantly different in length from the Ru(II)–bpy bond length
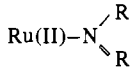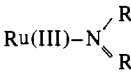
in $Ru(bpy)_3^{2+}$ (2.056 (6) Å). Yet the Ru(II)–pz bond in I (2.006 (6) Å) is 0.05 Å shorter than the Ru(II)–isn bond in the closely related complex *cis*-$Ru(NH_3)_4(isn)_2^{2+}$. A gradual increase in the Ru(II)–L bond length in the series $Ru(NH_3)_5L^{2+}$, $Ru(NH_3)_4L_2^{2+}$, etc. might have been expected from the following line of reasoning. Although the combination Ru(II)–L tends to form a strong (short) bond by virtue of π–d to L–π^* back-donation (present in addition to the strong σ component), binding of L to Ru(II) diminishes the

(19) Swanson, B. I.; Hamburg, S. I.; Ryan, R. R. *Inorg. Chem.* **1974**, *13*, 1685.

Table VII. Ru–N Bond Lengths in Ruthenium(II) and -(III) Amine Complexes[a]

complex	bond length, Å	ref
Ru(II)–NR$_3$		
Ru(NH$_3$)$_6$$^{2+}$	2.144 (4)	b
[Ru(NH$_3$)$_5$]$_2$N$_2$$^{4+}$	cis: 2.12	c
	trans: 2.02 (1)	
Ru(NH$_3$)$_5$NO^{3+}	2.10 (1) (av)	d
Ru(NH$_3$)$_5$pz^{2+}	2.155 (6) (av)	
Ru(en)$_2$(N$_3$)N$_2$$^+$	2.125 (19) (av)	i
Ru(NH$_3$)$_5$NO$_2$$^+$	cis: 2.131, 2.123	j
	trans: 2.199	
Ru(NH$_3$)$_4$(SO$_2$)Cl$^+$	2.127 (7) (av)	k
cis-Ru(NH$_3$)$_4$(isn)$_2$$^{2+}$	ax: 2.143 (5)	e
	trans: 2.170 (6)	
Ru(II)–N$\diagup^R_{\diagdown R}$		
Ru(NH$_3$)$_5$pz^{2+}	2.006 (6)	
cis-Ru(NH$_3$)$_4$(isn)$_2$$^{2+}$	2.060 (4) (av)	e
[Ru(py)$_4$]$_2$C$_2$O$_4$$^{2+}$	2.08 (av)	h
Ru(py)$_6$$^{2+}$	2.12 (1) (av)	m
Ru(bpy)$_3$$^{2+}$	2.056 (6)	n
Ru(III)–NR$_3$		
Ru(NH$_3$)$_6$$^{3+}$	2.104 (4)	f
Ru(en)$_3$$^{3+}$	2.11 (1) (av)	h
[Ru(NH$_3$)$_5$]$_2$(S$_2$$^{2-}$)$^{4+}$	cis: 2.12 (av)	g
	trans: 2.18 (av)	
Ru(NH$_3$)$_5$pz^{3+}	2.112 (7) (av)	
cis-Ru(NH$_3$)$_4$(isn)$_2$$^{3+}$	2.125 (7) (av)	e
Ru(III)–N$\diagup^R_{\diagdown R}$		
Ru(NH$_3$)$_5$pz^{3+}	2.076 (8)	
cis-Ru(NH$_3$)$_4$(isn)$_2$$^{3+}$	2.099 (4) (av)	e
trans-Ru(bpy)$_2$(OH)(H$_2$O)$^{2+}$	2.090 (3)	l
	2.099 (3)	
[Ru(bpy)$_2$NO$_2$]$_2$O^{2+}	2.077 (14) (av)	o

[a] Abbreviations: pz, pyrazine; isn, isonicotinamide; en, ethylenediamine; py, pyridine; av, average; bpy, 2,2′-bipyridine.
[b] Stynes, H. C.; Ibers, J. A. *Inorg. Chem.* **1971**, *10*, 2304.
[c] Treitel, I. M.; Flood, M. T.; Marsh, R. E.; Gray, H. B. *J. Am. Chem. Soc.* **1969**, *91*, 6512. [d] Bottomley, F. *J. Chem. Soc., Dalton Trans.* **1974**, 1600. [e] Richardson, D. E.; Walker, D. D.; Sutton, J. E.; Hodgson, K. O.; Taube, H. *Inorg. Chem.* **1979**, *18*, 2216. [f] Peresie, H. J.; Stanko, J. A. *Chem. Commun.* **1970**, 1674. [g] Elder, R. C.; Trkula, M. *Inorg. Chem.* **1977**, *16*, 1048. [h] Cheng, P. T.; Loescher, B. R.; Nyburg, S. C. *Ibid.* **1971**, *10*, 1275. [i] Davis, B. R.; Ibers, J. A. *Ibid.* **1970**, *9*, 2768. [j] Bottomley, F. *J. Chem. Soc., Dalton Trans.* **1972**, 2148. [k] Vogt, L. H.; Katz, J. L.; Wiberley, S. W. *Inorg. Chem.* **1965**, *4*, 1157. [l] Durham, B.; Wilson, S. R.; Hodgson, D. J.; Meyer, T. J. *J. Am. Chem. Soc.* **1980**, *102*, 600. [m] Templeton, J. L. *Ibid.* **1979**, *101*, 4906. [n] Rillema, D. P.; Jones, D. S.; Levy, H. *J. Chem. Soc., Chem. Commun.* **1979**, 849. [o] Phelps, D. W.; Kahn, M.; Hodgson, D. J. *Inorg. Chem.* **1975**, *14*, 2486.

π-electron density on the metal center and so should lower its ability to back-donate to a second (or third etc.) π-acceptor ligand. The bond length increase on going from Ru(NH$_3$)$_5$pz^{2+} to cis-Ru(NH$_3$)$_4$(isn)$_2$$^{2+}$ bears out this notion, but the similarity of the bond lengths in Ru(bpy)$_3$$^{2+}$ and cis-Ru(NH$_3$)$_4$(isn)$_2$$^{2+}$ does not. A possible explanation is that the Ru–isn bond is lengthened to accommodate steric requirements in the cis complex. The Ru(II)–L bond lengths in trans-Ru(NH$_3$)$_4$(isn)$_2$$^{2+}$ or cis-Ru(NH$_3$)$_4$bpy^{2+} would be of interest in this context.

The structures of the mononuclear species I and II provide a reference point for discussion of the mixed-valence complex [(NH$_3$)$_5$Ru]$_2$pz^{5+} (III).[20] The physical and chemical prop-

(20) Creutz, C.; Taube, H. *J. Am. Chem. Soc.* **1969**, *91*, 3988. Creutz, C.; Taube, H. *Ibid.* **1973**, *95*, 1086.

erties of this species have been interpreted in terms of a valence-trapped[11,21] Ru(II)–Ru(III) complex[22–27] and, alternatively, in terms of equivalent Ru(II^1/$_2$) sites.[28,29] The structural study of Beattie et al.[30] provides evidence for the latter model and yields the following bond lengths (Å): Ru–pz, 2.006 (6); Ru–NH$_3$, 2.127 (7) (trans to pz), 2.122 (5), 2.098 (5). For the (hypothetical) valence-trapped ion (NH$_3$)$_5$Ru^{II}–pz–Ru^{III}(NH$_3$)$_5$$^{5+}$, in which electron delocalization between the metal sites is absent, Ru–pz bond lengths of 2.01 and 2.08 Å for the Ru(II) and Ru(III) sites, respectively, would be expected from our results for I and II. Similarly the Ru–NH$_3$ bond lengths at the two sites would be expected to differ by $\sim$0.04 Å. For a delocalized ion, equivalent metal sites with metal–ligand bond lengths intermediate between those characteristic of Ru(II) and Ru(III) (e.g., Ru–pz $\approx$ 2.03 Å, Ru–NH$_3$ $\approx$ 2.12 Å) might have been anticipated. The observed Ru–pz bond length in the binuclear ion is thus much shorter than expected from these considerations.

The magnitude of the bond length changes associated with the oxidation or reduction of a metal complex, as well as the overall size of the complex, is an important parameter in determining the *rate* of the electron-transfer process. The free energy barrier to an electron-exchange process (ΔG^*) arises from the requirement that rearrangement of the nuclei and solvent precede electron transfer and is given by eq 1–3,[8,9]

$$\Delta G^* = \Delta G^*_{in} + \Delta G^*_{out} \qquad (1)$$

$$\Delta G^*_{in} = \left(\frac{6}{2}\right)\frac{f_1 f_2}{f_1 + f_2}(a_1 - a_2)^2 \qquad (2)$$

$$\Delta G^*_{out} = \frac{e^2}{4}\left(\frac{1}{a_1} + \frac{1}{a_2} - \frac{1}{d}\right)\left(\frac{1}{n^2} - \frac{1}{D_s}\right) \qquad (3)$$

where ΔG^*_{in} arises from inner-sphere coordination sphere distortions of the (six-coordinate) oxidized and reduced complexes which have metal–ligand bond lengths a_1 and a_2 and metal–ligand force constants f_1 and f_2, respectively. ΔG^*_{out} arises from reorganization of the medium (solvent) of static dielectric constant D_s and optical dielectric constant n^2. The reactants are separated by the distance d. (Equations 1–3 are for the case when the transition state for electron transfer has bond lengths and force constants given by the averaged parameters of the reactants.)

The fact that only rather small inner-sphere distortions ($<$0.05 Å on the average) accompany the rapid electron-transfer reactions of ruthenium(II) and -(III) ammines related to I and II has been discussed by Brown and Sutin,[10,31] who showed that ΔG^*_{out} is the dominant term for complexes of this type. Valence-trapped mixed-valence ions manifest new absorption features[11,21] (intervalence charge-transfer or metal-to-metal charge-transfer absorptions) whose energy E_{op} is related to the barrier for the electron-transfer process (E_{op} = $4\Delta G^*$)[11] and so, again, to the metal–ligand bond lengths in the two oxidation states. This application of crystallographic data has also been discussed for [Ru(NH$_3$)$_5$]$_2$(4,4′-bpy)$^{5+}$ for which I and II are expected to provide a good model.[32]

(21) Robin, M. B.; Day, P. *Adv. Inorg. Chem. Radiochem.* **1967**, *10*, 247.
(22) Mayoh, B.; Day, P. *J. Am. Chem. Soc.* **1972**, *94*, 2885.
(23) Creutz, C.; Good, M. L.; Chandra, S. *Inorg. Nucl. Chem. Lett.* **1973**, *9*, 171.
(24) Citrin, P. H. *J. Am. Chem. Soc.* **1973**, *95*, 6472.
(25) Elias, J. H.; Drago, R. *Inorg. Chem.* **1972**, *11*, 415.
(26) Strekas, T. C.; Spiro, T. G. *Inorg. Chem.* **1976**, *15*, 974.
(27) Bunker, B. C.; Drago, R. S.; Hendrickson, D. N. Kessell, S. L. *J. Am. Chem. Soc.* **1978**, *100*, 3805.
(28) Beattie, J. K.; Hush, N. S.; Taylor, P. R. *Inorg. Chem.* **1976**, *15*, 992.
(29) Hush, N. S. *Chem. Phys.* **1975**, *10*, 361.
(30) Beattie, J. K.; Hush, N. S.; Taylor, P. R.; Raston, C. L.; White, A. H. *J. Chem. Soc., Dalton Trans.* **1977**, 1121.
(31) Sutin, N. In "Tunneling in Biological Systems"; Chance, B., DeVault, D. C., Frauenfelder, H., Marcus, R. A., Schrieffer, J. R., Sutin, N., Eds.; Academic Press: New York, 1979; p 201.
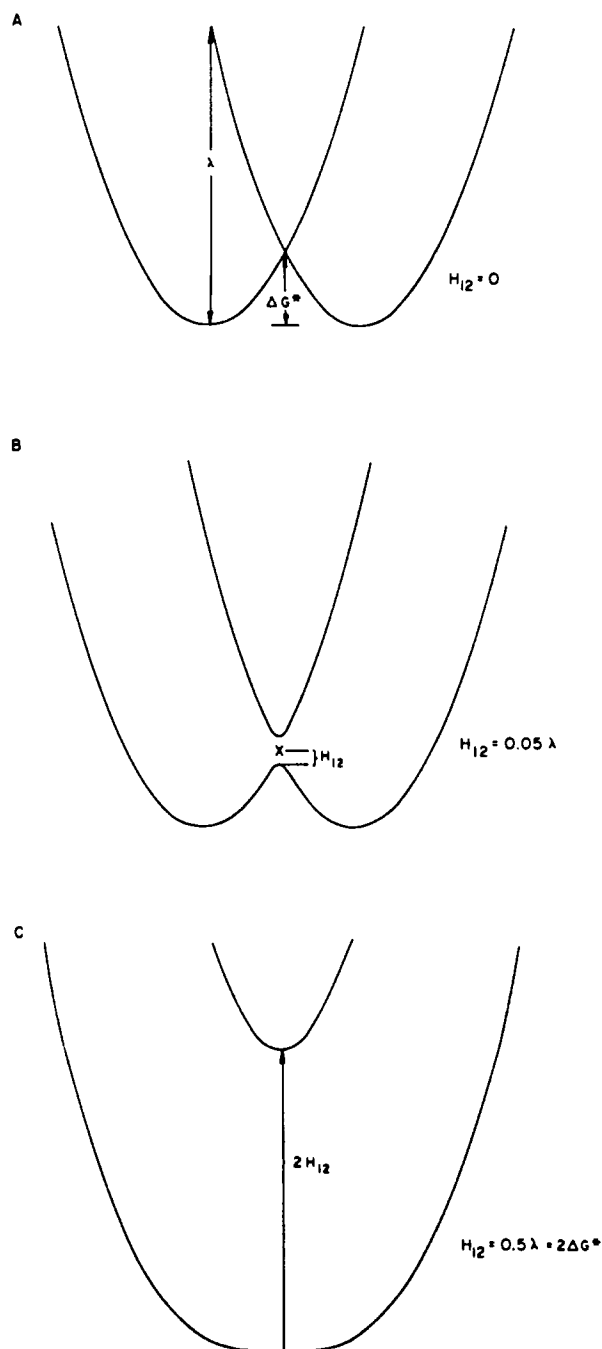
Figure 3. Potential energy of mixed-valence ions, i.e., $(NH_3)_5$-$Ru^{II}pzRu^{III}(NH_3)_5^{5+}$ (left-hand side) and $(NH_3)_5Ru^{III}pzRu^{II}(NH_3)_5^{5+}$ (right-hand side), as a function of nuclear configuration and H_{12}: (A) the resonance energy H_{12} between the Ru sites is zero, and the thermal barrier to electron transfer ΔG^* is $\lambda/4$; (B) introduction of a small H_{12} lowers the electron-transfer barrier by H_{12}; (C) when $H_{12} \geq \lambda/2$ or $2\Delta G^*$, the lower surface contains a single minimum and the mixed-valence ion is delocalized.

The same size factors arise in a final context in determining the nature of the electronic ground states of mixed-valence ions such as III. In the limit of zero interaction between the Ru(II) and Ru(III) metal centers the ion III would be expected (as discussed above) to contain different metal sites with the Ru(II) and Ru(III) sites resembling I and II, respectively, in dimensions. The sites may interchange via an electron-exchange process to which there is a kinetic barrier given by eq 1–3. This is shown in Figure 3A, a plot of potential energy of the binuclear ion as a function of nuclear configuration. The

left-hand parabola has the Ru(II) site on the left-hand side of the molecule; the right-hand parabola has the Ru(II) site on the right-hand side of the molecule. The potential energy at the intersection of the curves defines the classical thermal barrier to electron exchange ΔG^*. At the intersection the binuclear complex and the surrounding medium have undergone rearrangement to a relatively symmetric structure. In the simplest case ($f_1 = f_2$) the Ru–pz bond lengths are the same at both metal centers, as are the Ru–NH$_3$ distances. The energy of the electron at either site is identical with that at the other. Thus the transition state for the electron exchange in a localized mixed-valence complex is a delocalized mixed-valence complex. The vertical distance from the minimum of the left-hand curve to that of the right-hand curve gives E_{op} ($= 4\Delta G^*$). (This is the λ of Marcus and χ of Hush.) When moderate electron delocalization between the two sites occurs (Figure 3B), the curves are split at the intersection by $2H_{12}$ (where H_{12} is the resonance energy) and the thermal barrier to the electron exchange is diminished by H_{12}. If the resonance energy is sufficiently large (Figure 3C), the barrier to the exchange process vanishes and the mixed-valence ion becomes delocalized. The lower potential energy surface features a single minimum, that for a delocalized ion containing equivalent metal sites. This species manifests a new electronic transition at $h\nu_{max} = 2H_{12}$. Hush[28,29] has given a detailed discussion of the transition from the valence-trapped to the delocalized ground state for mixed-valence ions and concluded that the transition to a single minimum occurs when $H_{12} = 2\Delta G^* = \lambda/2$.

The nature of the electronic structure of III with reference to the model in Figure 3 has been examined through the shape and position of its mixed-valence transition observed at ~1570 nm[26] in solids and solutions at room temperature. By fitting solid-state spectra of a halide salt of III to a delocalized model,[28] Beattie et al.[28] obtained $H_{12} = 0.39$ eV and $\Delta G^* = 0.12$ eV (for the hypothetical $H_{12} = 0$). Piepho et al.[33] derived a model in which the potential energy surface of III in water at 25 °C features shallow double minima with $H_{12} = 0.37$ eV and $\Delta G^* = 0.23$ eV (for the hypothetical $H_{12} = 0$) and concluded that III is essentially delocalized under these conditions as well. The agreement between the H_{12} values from the two studies is striking, and the differing values obtained for ΔG^* are readily interpreted in terms of eq 1–3. While H_{12} is a function of the electronic properties of III and should be medium independent, the magnitude of ΔG^* should be a function of the medium in which the complex is studied. From eq 3, ΔG^* should be much greater in a medium of high dielectric constant (water) than in a solid of low dielectric constant (a chloride or bromide salt). In fact, knowledge of the structures of I and II and the use of eq 1–3 permit ΔG^* for the two media to be estimated numerically as follows. The value of ΔG^*_{in}, which is expected to be medium invariant, is found to be 1.0 kcal mol^{-1} from the metal–ligand bond lengths found for I and II and estimated metal–ligand force constants discussed elsewhere.[32] A value of $\Delta G^*_{out} = 6.4$ kcal mol^{-1} is obtained for water as solvent, but ΔG^*_{out} is much smaller, ~2 kcal mol^{-1}, in the low-dielectric-constant medium halide salt. Total ΔG^* values of 7.4 kcal mol^{-1} (0.32 eV) and 3 kcal mol^{-1} (0.13 eV) are thus obtained for water and the halide salt, respectively. These are in rather good agreement with the ΔG^* values of 0.23[33] and 0.12 eV[28] obtained from the spectral fits for water and the solid, respectively.

In summary, these considerations lead to a consistent picture of the nature of III. The delocalization energy arising from interaction between zero-order Ru(II) and -(III) sites is 0.4 eV in III. In the crystalline state, a "delocalization barrier"

(32) Creutz, C. *Inorg. Chem.* **1978**, *17*, 3723.

(33) Piepho, S.; Krausz, E. R.; Schatz, P. N. *J. Am. Chem. Soc.* **1978**, *100*, 2996.

$(2\Delta G^*)$ of ~ 0.2 eV is overcome so that the ion's ground state is delocalized. In water the barrier to delocalization is much greater (calculated 0.64 eV, observed[33] 0.46 eV), but the ion remains essentially delocalized.[33] It is difficult to avoid the conclusion that, could the magnitude of H_{12} be reduced or should a medium of higher dielectric constant be employed for study of III or could a sufficiently large ΔG^*_{in} be introduced (so that $\Delta G^* \gg 0.2$ eV), III would exhibit the properties of a localized mixed-valence ion. Indeed such properties have been observed for analogous diruthenium complexes in which the metal–metal separation is greater than in III and H_{12} is consequently smaller.[12,32]

Contribution from the Departments of Chemistry, University of Illinois, Urbana, Illinois 61801, and University of Colorado, Boulder, Colorado 80309

Crystal Structure and Solution Dynamics of (μ-H)Os₃(CO)₁₀(μ-η²-CPh=CHPh)

A. D. CLAUSS,[1a] M. TACHIKAWA,[1a] J. R. SHAPLEY,*[1a] and C. G. PIERPONT*[1b]

Received August 29, 1980

The hydridostilbenyl complex HOs₃(CO)₁₀(CPh=CHPh) has been synthesized from the reaction of H₂Os₃(CO)₁₀ with excess diphenylacetylene at room temperature. The molecular structure of the stilbenyl complex is reported and compared to the structures of other alkenyltriosmium complexes. Crystals of HOs₃(CO)₁₀(CPh=CHPh) form in the space group $P2_12_12_1$ with $a = 11.521$ (2) Å, $b = 14.244$ (2) Å, $c = 31.695$ (4) Å, $V = 5201.3$ (10) Å³, ρ(obsd) = 2.64 (2) g cm⁻³, ρ(calcd) = 2.633 g cm⁻³, for mol wt 1031.0 and $Z = 8$. The molecule contains a triangular array of osmium atoms with the stilbenyl ligand bridging the Os(1)–Os(2) edge and forming a σ bond to Os(2) and a π bond to Os(1). All carbonyl ligands are terminally bound; Os(1) and Os(2) each have three carbonyls, whereas Os(3) has four carbonyls. The presence of a bridging hydride along the Os(1)–Os(2) edge was not detected directly but was supported by analysis of the carbonyl bond angles. The orientation of the alkenyl ligand in HOs₃(CO)₁₀(CPh=CHPh) differs from that observed in the previously characterized alkenyl compounds HOs₃(CO)₁₀(CH=CHR) (R = H, Et). The vinyl derivatives have been shown to have a structure in which Os(3) is syn with respect to the hydrogen atom on the α-carbon of the ligand. In contrast, the stilbenyl ligand is positioned so that Os(3) is anti with respect to the substituent on the α-carbon, which in this case is a phenyl group. Variable-temperature ¹³C NMR spectra of the carbonyl resonances of HOs₃(CO)₁₀(CPh=CHPh) revealed that the stilbenyl ligand is fluxional. The spectral behavior observed is consistent with a mechanism involving a facile interchange of the σ and π bonds between the bridged osmium atoms. Similar fluxional behavior was observed previously for the vinyl derivatives. The activation barrier (ΔG^*_c) for this rearrangement in the case of the stilbenyl ligand was found to be 11.3 kcal/mol compared to 10.3 kcal/mol for the vinyl ligand in HOs₃(CO)₁₀(CH=CH₂).

Introduction

Alkenyltriosmium compounds of the general formula HOs₃(CO)₁₀(CRCR'R'') demonstrate a variety of bonding modes that differ in the orientation of the alkenyl ligand with respect to the metal triangle. The unsubstituted complex HOs₃(CO)₁₀(CH=CH₂) and the closely related compound HOs₃(CO)₁₀(CH=CHEt) have been shown to have structure I.[2,3] The vinylic moiety in these compounds is an edge-

bridging ligand that forms a σ bond to one osmium atom and a π bond to the adjacent osmium atom. A quite different structure (II), in which the alkenyl ligand is coordinated to all three osmium atoms, has been found to occur in HOs₃(CO)₁₀(CCF₃CHCF₃).[4] On the other hand, for HOs₃(CO)₁₀(CHCHNEt₂), structure III is observed, in which the ligand is formally a 1,3 dipolar iminium ion (C⁻HCH=N⁺Et₂) coordinated as an edge-bridging substituted methylene moiety.[5]

We have previously made brief mention of the stilbenyl compound HOs₃(CO)₁₀(CPh=CHPh), which was isolated as an intermediate in the stoichiometric reduction of acetylene to *cis*-stilbene by H₂Os₃(CO)₁₀.[6] Significant differences in the IR (ν_{CO}) spectrum of HOs₃(CO)₁₀(CPh=CHPh) compared to the compounds HOs₃(CO)₁₀(CH=CH₂) and HOs₃(CO)₁₀(CH=CHEt)[7] prompted us to undertake a sin-

(2) Orpen, A. G.; Ricera, A. V.; Bryan, E. G.; Pippard, D.; Sheldrick, G. M.; Rouse, K. D. *J. Chem. Soc., Chem. Commun.* **1978**, 723.

(3) Guy, J. J.; Reichert, B. E.; Sheldrick, G. M. *Acta Crystallogr., Sect. B* **1976**, *B32*, 3319.

(4) Laing, M.; Sommerville, P.; Dawoodi, Z.; Mays, M. J.; Wheatley, P. J. *J. Chem. Soc., Chem. Commun.* **1978**, 1035.

(5) (a) Shapley, J. R.; Tachikawa, M.; Churchill, M. R.; Lashewycz, R. A. *J. Organomet. Chem.* **1978**, *162*, C39. (b) Churchill, M. R.; Lasewycz, R. A. *Inorg. Chem.* **1979**, *18*, 848.

(6) (a) Tachikawa, M.; Shapley, J. R.; Pierpont, C. G. *J. Am. Chem. Soc.* **1975**, *97*, 7172. (b) Characterization of HOs₃(CO)₁₀(CPh=CHPh) was also reported by Deeming et al.: Deeming, A. J.; Hasso, S.; Underhill, M. *J. Chem. Soc., Dalton Trans.* **1975**, 1614.

(7) HOs₃(CO)₁₀(CH=CH₂): IR (ν_{CO}, C₆H₁₂) 2110 w, 2066 vs, 2058 s, 2026 vs, 2014 m, sh, 1998 m, 1989 w, sh, 1984 w cm⁻¹. The other HOs₃(CO)₁₀(CH=CHR) derivatives have very similar IR spectra (see ref 6 and 8).

(1) (a) University of Illinois. (b) University of Colorado.